The Role of Al in Cross-Linking of Alkali-Activated Slag Cements

The role of Al in cross-linking of alkali-activated slag cements

Rupert J. Myers,[1] Susan A. Bernal,[1,2] John L. Provis,[1,2*]

John D. Gehman,[3,4] Jannie S.J. van Deventer[2,5]

[1] Department of Materials Science and Engineering, University of Sheffield, Sir Robert Hadfield Building, Mappin St, Sheffield S1 3JD, United Kingdom

[2] Department of Chemical and Biomolecular Engineering, The University of Melbourne, Victoria 3010, Australia

[3] School of Chemistry and Bio21 Institute, The University of Melbourne, Victoria 3010, Australia

[4] GehmanLab, Woodend, Victoria 3442, Australia

[5] Zeobond Pty Ltd, P.O. Box 23450, Docklands, Victoria 8012, Australia

* To whom correspondence should be addressed. Email j.provis@sheffield.ac.uk, phone +44 114 222 5490, fax +44 114 222 5493

Abstract

The structural development of a calcium (sodium) aluminosilicate hydrate (C-(N-)A-S-H) gel system, obtained through the reaction of sodium metasilicate and ground granulated blast furnace slag, is assessed by high resolution ^{29}Si and ^{27}Al MAS NMR spectroscopy during the first 2 years after mixing. The cements formed primarily consist of C-(N-)A-S-H gels, with hydrotalcite and disordered alkali aluminosilicate gels also identified in the solid product assemblages. Deconvolution of the ^{27}Al MAS

NMR spectra enables the identification of three distinct tetrahedral Al sites, consistent with the ^{29}Si MAS NMR data, where $Q^3(1Al)$, $Q^4(3Al)$ and $Q^4(4Al)$ silicate sites are identified. These results suggest significant levels of cross-linking in the C-(N-)A-S-H gel and the presence of an additional highly polymerized aluminosilicate product. The mean chain length, extent of cross-linking and Al/Si ratio of the C-(N-)A-S-H gel decrease slightly over time. The de-cross-linking effect is explained by the key role of Al in mixed cross-linked/non-cross-linked C-(N-)A-S-H gels, because the cross-linked components have much lower Al-binding capacities than the non-cross-linked components. These results show that the aluminosilicate chain lengths and chemical compositions of the fundamental structural components in C-(N-)A-S-H gels vary in a way that is not immediately evident from the overall bulk chemistry.

Keywords: Aluminosilicate gel, calcium silicate hydrate (C-S-H), blast furnace slag, ^{29}Si and ^{27}Al MAS NMR, nanostructural evolution

1. Introduction

Many modern cements contain Portland cement (PC) blended with Al-containing supplementary cementitious materials (SCMs).[1] The solid binders in these cements contain calcium aluminosilicate hydrate (C-A-S-H) gels with moderate Ca content (Ca/(Al+Si)≈1) rather than the more Ca-rich (1.5≤Ca/Si≤2) calcium silicate hydrate (C-S-H) gels that form as the primary reaction product in neat PC materials. To reduce complexities related to secondary phases in these materials, studies of C-A-S-H chemistry have often focused on laboratory-synthesized pastes with compositions in the CaO-SiO_2-Al_2O_3-H_2O(-Na_2O/K_2O) system,[2-5] and on alkali-activated slag (AAS) cements.[6-8]

AAS cements are now finding industrial application in the production of concretes with high mechanical performance, low life cycle CO_2 emissions relative to PC-based materials, and good durability.[9; 10] Understanding the durability of such concretes remains a key scientific challenge,

because durability is closely related to the chemistry and the pore network geometry of the solid binder.[11] Therefore, elucidation of the binder chemistry, and in particular the details of the C-A-S-H gel which is the key space-filling and strength-giving component, is essential.

It has been shown that the processes of incorporation of Al and alkalis in C-S-H gels are directly related,[12; 13] meaning that calcium (alkali) aluminosilicate hydrate (C-(N-)A-S-H) gels are formed in systems that are rich in both Al and alkalis (denoted 'N' to reflect the activators used in AAS, which are typically Na-based). This is also consistent with the increase in alkali uptake in systems with lower Ca/Si ratios through a valence compensation mechanism,[12] in which the charge imbalance created by Al/Si substitution or silanol deprotonation is balanced by positively-charged species in the interlayer.

The variable molecular structure of C-(N-)A-S-H gel, as well as the nanoparticulate nature of the gel formed through agglomeration of structural units around several nanometers in size,[14] results in a structure with limited long-range ordering. Elucidation of the structure of this phase in AAS cements and blended PC/Al-containing SCM materials challenging because of this high level of structural disorder, and also because the C-(N-)A-S-H gel almost always coexists with unreacted remnant precursor particles and secondary reaction products. Thus, important questions remain about its molecular chemistry, including the following possibilities:

i) the presence of cross-linked chains;[15-18]

ii) Al substitution into paired tetrahedra;[3; 5; 19]

iii) the role and importance of five-coordinated Al (denoted Al[5]).[2; 4; 20]

Various studies applying ^{29}Si magic angle spinning nuclear magnetic resonance (MAS NMR) and ^{27}Al MAS NMR spectroscopy to silicate-activated slag cements have been published,[7; 8; 15] but where deconvolution of the spectra has been undertaken, the contribution of unreacted slag is not always distinguished. Quadrupolar lineshapes are also not always used in deconvolutions of ^{27}Al MAS NMR

spectra, which greatly affects the calculated contributions of the different identifiable site environments.

Therefore, this study presents detailed ^{29}Si and ^{27}Al MAS NMR analysis of a sodium silicate-activated slag cement as a function of the time of curing, to clarify the complex relationship that exists between the chemical composition and nanostructure of C-(N-)A-S-H gels, and the solid phase assemblage in these materials. The spectra are deconvoluted with consideration of remnant unreacted slag particles and quadrupolar coupling effects, enabling quantification of the chemistry of the reaction products, with secondary phases identified by X-ray diffraction (XRD). Application of a model that represents the C-(N-)A-S-H gel as a mixture of non-cross-linked and cross-linked tobermorite-like structures[16] provides further information regarding the structure and chemical composition of this phase.

2. Experimental

2.1. Materials and sample preparation

Granulated blast furnace slag supplied by Zeobond Pty Ltd. (Australia) was used in this study, with a chemical composition as listed in Table 1, specific gravity of 2800 kg/m^3, Blaine fineness of 410 m^2/kg, and d_{50} = 15 μm according to laser granulometry (Malvern Mastersizer).

The alkali activator was prepared by dissolution of solid NaOH pellets (Sigma-Aldrich, Australia) into D grade (PQ, Australia) sodium silicate, to reach a solution modulus (SiO_2/Na_2O molar ratio) of 1.0. The overall molar Na_2O/Al_2O_3 ratio was fixed at 0.50, including Na supplied by the activator and the slag, corresponding to an overall activator dose of 8 g Na_2SiO_3 /100 g slag. Water was added to the activator to reach a water/binder (w/b) ratio of 0.40, which was then allowed to cool to room temperature prior to preparation of the specimens. Paste specimens were cured in sealed bags at 23°C until testing. Samples were crushed by hand before analysis.

2.2. Tests conducted

XRD was conducted using a Bruker D8 Advance instrument with Cu Kα radiation and a nickel filter. The tests were conducted with a step size of 0.020°, for a 2θ range of 5° to 70°.

Solid-state ^{29}Si MAS NMR spectra were collected at 119.1 MHz on a Varian VNMRS-600 (14.1 T) spectrometer using a probe for 4 mm o.d. zirconia (PSZ) rotors and a spinning speed (ν_R) of 10.0 kHz. The ^{29}Si MAS experiments employed a pulse width of 4 µs, a relaxation delay of 20 s, and 4096 scans. Solid-state ^{27}Al MAS NMR spectra were acquired at 156.3 MHz on the same instrument for the unreacted slag and samples cured for 1-180 days, with a pulse width of 0.5 µs, a relaxation delay of 2 s, and at least 1000 scans. All spectra were collected with a tip angle of 51°. Additional ^{27}Al MAS NMR spectra were acquired at 104.2 MHz on a Varian VNMRS 400 (9.4 T) spectrometer for the unreacted slag and the sample cured for 2 years with ν_R = 14 kHz, a pulse duration of 1 µs, recycle delay of 0.2 s and 7000 repetitions. ^{29}Si chemical shifts are referenced to external tetramethylsilane (TMS), and ^{27}Al chemical shifts are referenced to external 1.0 M aqueous $Al(NO_3)_3$ via internal referencing using the hydrotalcite peak at δ_{iso} = 9.68 ppm (the isotropic chemical shift), using the parameters C_Q = 1.2 MHz and η_Q = 0.8 as determined for a pure hydrotalcite sample (S.A. Walling and S.A. Bernal, unpublished data) and the calculation method reported in [21].

Deconvolutions of the ^{29}Si MAS NMR spectra were performed using the minimum number of component peaks needed to describe the spectra. The spectra were manually fitted with Gaussian functions, with the full width at half height (FWHH) of each component peak constrained to be <10 ppm, and peaks assigned to connectivity states based on information available in the literature for cements,[13; 22] zeolites,[23] and silicate-activated slag cements.[24] Peak positions and widths for each identified species were held constant throughout the deconvolution process. The component peaks

assigned to the remnant slag were rescaled vertically by a single factor in each spectrum, to provide the appropriate lineshape in the corresponding regions of the spectra.

^{27}Al MAS NMR spectra were deconvoluted manually using Dmfit[25] and the (Czjzek) Gaussian Isotropic Model[26; 27] to model quadrupolar peak shapes. The secondary reaction products identified by XRD were quantified in the spectra using component peaks consistent with the literature.[20; 28] Quadrupolar coupling parameters (C_Q) from the literature were used to define peak shapes, as outlined in section 3.3. Full details regarding spectral quantification are provided in Appendix A. Isotropic chemical shifts (δ_{iso}) were calculated for the peaks in the deconvoluted spectra using the method described in [20], using the observed chemical shift (δ_{obs}) values determined here.

3. Results and discussion

3.1. X-ray diffraction

The XRD results are presented in Figure 1. There is a small quantity of åkermanite ($Ca_2MgSi_2O_7$, PDF#00-035-0592) in the remnant slag.[24] Peaks corresponding to a poorly crystalline tobermorite-like C-S-H type gel are observed (similar to $Ca_5(Si_6O_{16})(OH_2)$, PDF#01-089-6458), consistent with the literature for sodium silicate-activated slag cements.[24; 29; 30] Hydrotalcite ($Mg_6Al_2(CO_3)(OH)_{16}{\cdot}4H_2O$, PDF#00-041-1428) is also identified as a reaction product, which is consistent with other studies[6; 24; 30-33] of AAS with significant magnesium content. The increase in intensity of the main hydrotalcite peak (11.4° 2θ) with increasing time of curing, and similarly the peak of the C-S-H type gel at 29.5° 2θ, are consistent with the activation reaction continuing with age.

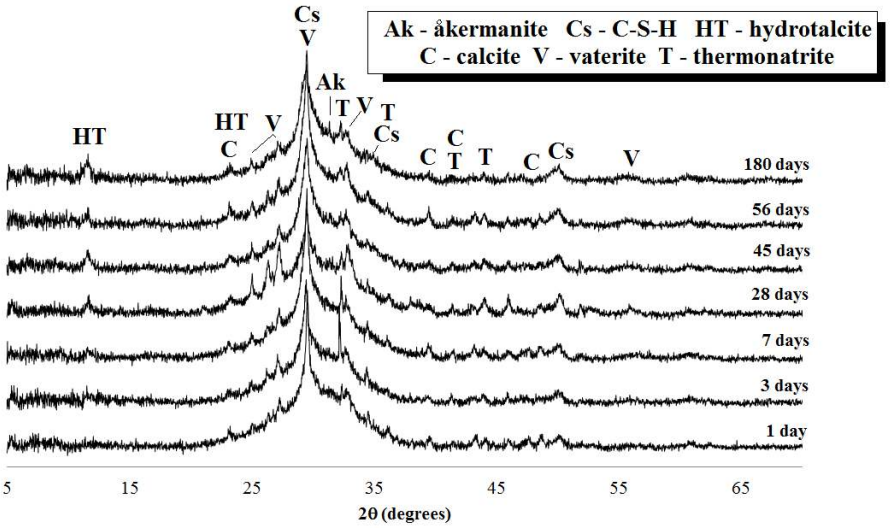

Figure 1. Cu Kα diffractograms of the Na_2SiO_3-activated slag cement as a function of curing time.

Minor traces of calcite (PDF#01-083-0577) and vaterite (PDF#01-074-1867), along with thermonatrite ($Na_2CO_3 \cdot H_2O$, PDF#01-072-0578), are associated with slight atmospheric carbonation of the specimens during sample preparation and analysis.

3.2. ^{29}Si MAS NMR spectroscopy

The ^{29}Si MAS NMR spectrum of the unreacted slag (Figure 2) is in good agreement with results for a melilite-type glass,[34] consistent with the identification of åkermanite by XRD in the slag used in this study. The activation of the slag precursor results in the formation of at least three intense bands at -80 ppm, -83 ppm and -86 ppm in the ^{29}Si MAS NMR spectra (Figure 2), which are assigned to Q^1, Q^2(1Al) and Q^2 sites respectively in the C-(N-)A-S-H gel.[7; 17; 22; 24; 35]

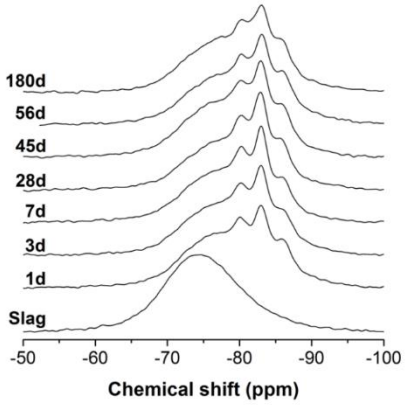

Figure 2. ^{29}Si MAS NMR spectra of the Na_2SiO_3-activated slag cement as a function of curing time.

A reduction in the intensity of the band corresponding to the remnant slag is observed, which is attributed to the progress of the activation reaction. A Q^0 site at -74 ppm and an additional Q^1 site at -78 ppm (Figure 3 and Appendix B), distinct from the site at -80 ppm, were assigned because the lineshapes of the experimental spectra in the less negative chemical shift region (> -80 ppm) could not all be matched using a single peak attributed to the remnant slag, or to any two out of the three aforementioned components, under the deconvolution constraints applied here.

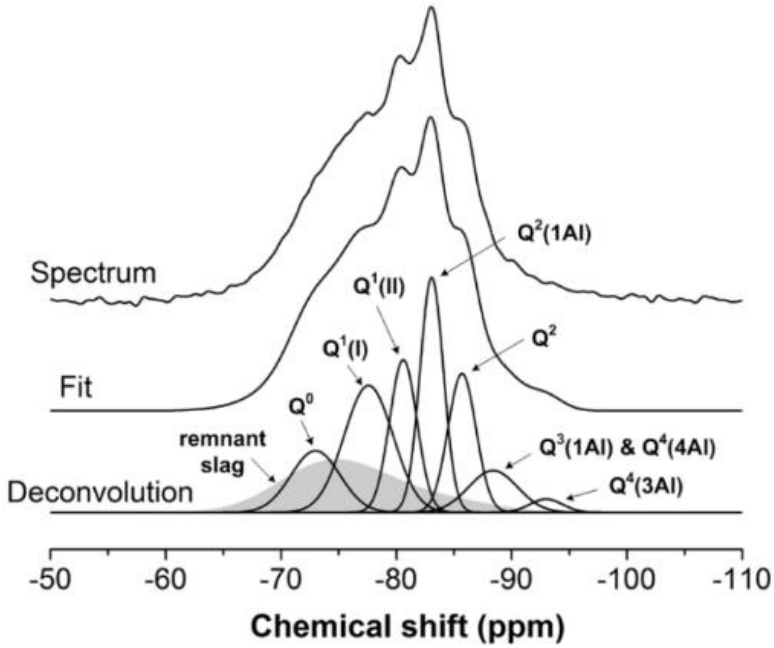

Figure 3. Deconvoluted ^{29}Si MAS NMR spectrum of the Na_2SiO_3-activated slag cement cured for 180 days. The dark grey band represents the contribution of the remnant slag, which is directly scaled from the spectrum collected for the unreacted slag. Deconvolutions of the spectra obtained at the other ages studied are given in Appendix B.

The identification of two non-equivalent Q^1 environments in the binder is consistent with molecular dynamics studies of non-isolated C-S-H gels, which identified significant differences between the shielding behavior (and hence chemical shifts) of Q^1 sites charge-balanced by Ca^{2+} or H^+ (Figure 4).[36] Charge-balancing by Na^+ is also likely in the systems studied here. There are many possible combinations of potential charge-balancing species for Q^1 sites; these are represented in the deconvolutions by two Gaussian peaks as this is the smallest number of peaks which can adequately represent this region of the spectra, while acknowledging that there are in fact many more chemically distinct sites than this within the material. For the purposes of the analysis, these peaks are labelled Q^1(I) and Q^1(II), where it is likely that Q^1(I) at -78 ppm corresponds generally to sites connected to charge-balancing atoms (e.g. H^+, Na^+) with less strong positive charges than those associated with Q^1(II) at -80 ppm (e.g. Ca^{2+}). It is also noted that the differences in calculated chemical shift values for Q^2 units as a function of charge-balancing species are much less pronounced,[36] supporting the assignment of a single site for structurally-similar Q^2 species in the deconvolutions. The site environments marked in Figure 3 are shown in Figure 5.

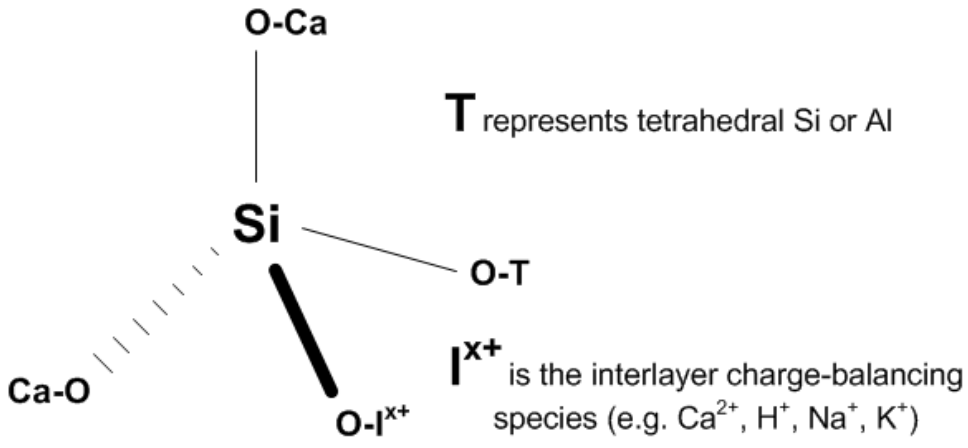

Figure 4. Illustration of the variety of charge-balancing species which can bind to a Q^1 site in C-(N-)A-S-H gel, leading to multiple peaks in the spectra. The Ca species are located in the Ca-O sheets.

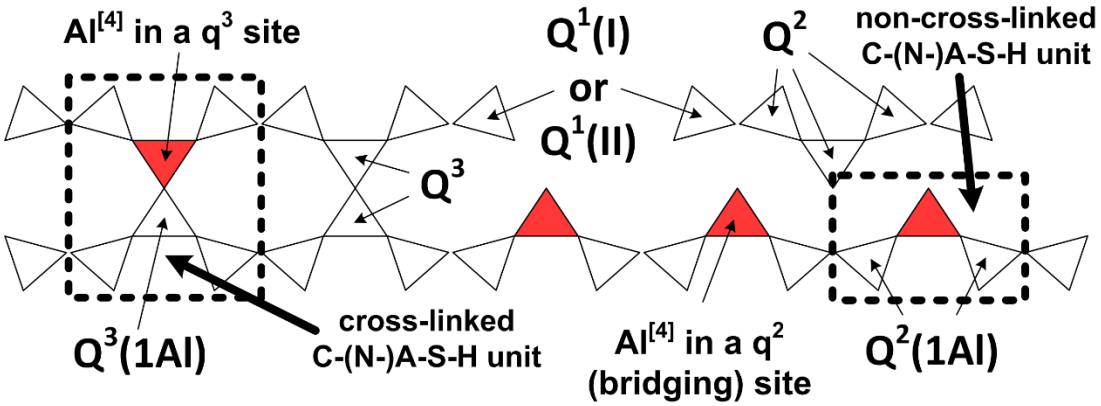

Figure 5. Schematic representation of cross-linked and non-cross-linked chain structures which represent the generalized structure of C-(N-)A-S-H type gels. The red and white tetrahedra are aluminate and silicate species respectively.

Significant non-zero intensity at approximately -91 ppm becomes apparent at 56 and 180 days of curing (Figure 3 and Appendix B). This signal is assigned in part to Q^4(3Al) and Q^4(4Al) in a disordered aluminosilicate product, tentatively proposed here to resemble an alkali aluminosilicate (hydrate) (N-A-S(-H)) gel, and in part to Q^3(1Al) units in C-(N-)A-S-H gel. In the deconvolutions here, a combined band for Q^4(4Al)/Q^3(1Al) and a peak for Q^4(3Al) are positioned at -89 ppm and -93 ppm respectively, consistent with a recent structural model and interpretation of ^{29}Si MAS NMR results,[16] without precluding the presence of a small concentration of Q^3 units that could also be present at approximately -93 ppm in AAS cements.[5; 15] These assignments are also chosen because this is the minimum number of peaks that can satisfactorily fit the lineshape of the spectra in this chemical shift range.

Recently,[16] a generalized model for Al-substituted, alkali charge-balanced cross-linked and non-cross-linked tobermorite-like structures, the 'Cross-linked Substituted Tobermorite Model' (CSTM), was developed and applied to describe the C-(N-)A-S-H gels present in AAS cements. It was found that a mixture of cross-linked and non-cross-linked tobermorite-like C-(N-)A-S-H and established secondary product phases could not fully explain the chemistry of the sodium-silicate activated slag binder alone, due to the inherent structural constraints of C-(N-)A-S-H gels, suggesting the presence of an additional

Al-containing activation product. If this product contains aluminosilicate species contributing to the intensity of the -89 ppm and -93 ppm bands in ^{29}Si MAS NMR spectra, these are most likely Q^4(4Al) and Q^4(3Al) units respectively and the additional product is probably a N-A-S(-H) gel with Si/Al ≤ 1.2.[37] Therefore, the assignment of the -93 ppm peak to Q^4(3Al) in a N-A-S(-H) gel, rather than Q^3 in C-(N-)A-S-H, is necessary to satisfy the structural constraints of mixed non-cross-linked/cross-linked tobermorite-like C-(N-)A-S-H gels.[16]

The small band at -89 ppm (Figure 3) increases slightly in intensity with curing time. This peak is attributed to cross-linked Q^3(1Al) silicate sites in the C-(N-)A-S-H gel, as well as Q^4(4Al) in the N-A-S(-H) gel, which is again consistent with the structural model and interpretation of ^{29}Si MAS NMR results recently proposed by Myers et al.,[16] and with previous studies on sodium silicate-activated and sodium carbonate-activated slag cements.[17; 24; 32; 38] It is necessary here to attribute part of this band to Q^4(4Al), because the inclusion of Q^4(3Al) sites into the ^{29}Si MAS NMR spectral deconvolution results requires the presence of additional Q^4 type units; there is no aluminosilicate gel which consists solely of Q^4(3Al) sites.[37] It was previously shown[37] that Al-rich (Si/Al ≤ 1.2) geopolymers contain almost exclusively Q^4(3Al) and Q^4(4Al) units. This strongly supports the inclusion of Q^4(3Al) and Q^4(4Al) into the ^{29}Si MAS NMR spectral deconvolutions here, and indicates that AAS cements may contain disordered nanoparticulate, possibly zeolite-like, products similar to the N-A-S(-H) gels formed through activation of low-calcium aluminosilicate precursors.[39; 40] This assignment is also consistent with the observation of zeolites in some AAS cements after extended curing periods.[41-43] The assigned Q^4(3Al) and Q^4(4Al) peaks may alternatively be attributed to Q^4(*m*Al)-containing aluminosilicate gels formed through degradation of C-(N-)A-S-H during superficial carbonation of the specimen,[24] however the XRD results (Figure 1) do not show the systematic increase in carbonation with curing time needed for full consistency with this assignment (Q^4(*m*Al) sites are only apparent at 56 and 180 days here).

Quantification of ^{29}Si sites, determined through deconvolution of the ^{29}Si MAS NMR spectra as a function of curing duration, is reported in Table 2, with full deconvoluted spectra presented as

Supporting Information in Appendix B. As much as 54% of the slag is seen to have reacted within the first day of curing, and 77% after 56 days, assuming congruent dissolution of the slag and complete uptake of the silica supplied by the activator into the solid binder (Electronic Supporting Information, Appendix A). The reaction extent of the slag identified by this method is greater than was determined by SEM image analysis for slag particles (of unspecified fineness) reacted with a $Na_2SiO_3 \cdot 5H_2O$ activator (~3 g Na_2O equivalent/100 g slag) at w/b = 0.40 and 23°C,[18] which gave hydration degrees of approximately 40% at 1 day and 55% at 56 days. Similar or lower extents of reaction have been observed for AAS cements activated at 20°C using sodium silicate and NaOH solutions (~3 g Na_2O equivalent/100 g slag),[44] and in water-activated blended slag/PC materials,[45] suggesting that the slag precursor used here is more reactive under alkaline activation conditions compared to the slags used in those studies.

A single band was fitted for Q^2 sites despite the known ~2 ppm difference between Si present in paired (Q^2_p) environments relative to bridging (Q^2_b) sites within C-S-H type gels,[5] because assigning peaks for both Q^2_b and Q^2_p sites would lead to an unconstrained deconvolution procedure.

Significant amounts of Q^2(1Al) are present, indicating high levels of Al substitution in the C-(N-)A-S-H gel. The presence of Q^3(1Al) units also shows that the C-(N-)A-S-H gel is significantly cross-linked. Constant non-zero quantities of Q^4(3Al) and Q^4(4Al) sites are resolved at 56 and 180 days of curing. Quantification of the Q^4(4Al) site was performed assuming that the additional N-A-S(-H) gel only contains Q^4(3Al) and Q^4(4Al) units at an Si/Al ratio of 1.2, and the remainder of the intensity of the peak at -89 ppm was assigned to Q^3(1Al). This Si/Al ratio was selected as it is at the upper end of the range in which an aluminosilicate gel would be comprised almost entirely of Q^4(3Al) and Q^4(4Al) units;[37,46] a higher Si/Al ratio would also require the presence of Q^4(2Al) sites, and these are not evident in the spectra here. Full details regarding the assignment of the bands at -93 ppm and -89 ppm are provided in Electronic Supporting Information, Appendix C.

The evolving structure of the C-(N-)A-S-H gel is represented in Figure 6, by normalizing the contributions of reaction products to sum to 100%.

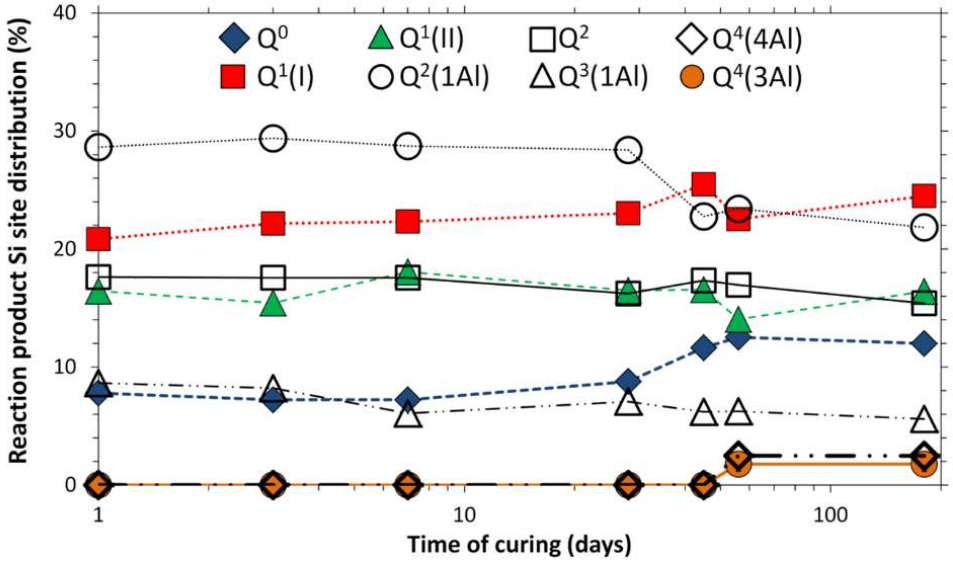

Figure 6. Deconvolution results of the ^{29}Si MAS NMR spectra, normalized to the total intensity of the reaction products.

The normalized ^{29}Si MAS NMR spectral deconvolutions (Figure 6) show that the relative concentrations of the Q^1(II) and Q^2 sites do not vary greatly from 1 to 180 days of curing. An increasing trend in the relative concentrations of Q^0 and Q^1(I) sites, and a decreasing trend in the relative concentrations of Q^2(1Al) and Q^3(1Al) sites, are observed over the entire range of curing ages studied. The increasing prevalence of Q^1(I) sites, and the corresponding reduction in the concentrations of Q^2(1Al) and Q^3(1Al) units, are associated with the gradual transformation of the C-(N-)A-S-H gel to structures with lower mean chain length (MCL; see section 3.4) and increasing secondary product formation (Figure 1 and section 3.3) as the time of curing increases. This reduction in MCL can also potentially be reconciled with the relative increase in percentage of the bands at -74 ppm (tentatively assigned to Q^0 here) if these peaks represent surface-bound Q^0 units, as increasing the relative surface area of C-(N-)A-S-H gel can be consistent with a reduction in MCL. The decreasing trend in the concentration of Q^3(1Al) sites (in cross-linked C-(N-)A-S-H gel) is also consistent with the observed decreasing relative percentage of Q^2(1Al) sites, because a reduction in Q^3(1Al) necessitates a lower concentration of

Q^2(1Al) (Figure 5). Therefore, these results indicate that the degree of cross-linking of the C-(N-)A-S-H gel decreases over time, which is to some extent a counterintuitive result, and which will be explored in more detail in section 3.4 below.

The Q^0 site at -74 ppm is assigned to partially hydrated silicate monomers or Q^0 components of the remnant slag that have not reacted congruently without precluding the possibility that Q^1(1Al) species contribute to a small fraction of this peak. The presence of Q^1(1Al) in the ^{29}Si MAS NMR spectra would imply Al substitution in paired tetrahedral sites in the C-(N-)A-S-H gel, given that tetrahedral site vacancies only occur in the bridging position (as described by 3*n*-1 chain length models for C-(N-)A-S-H [47]). Al substitution into paired sites is not expected because atomistic simulations of Al-substituted pentameric chains in environments representative of 14 Å tobermorite,[48] in sheets representing 14 Å tobermorite,[19] and in isolated chains,[49] have shown significant energetic preferences for Al substitution in bridging sites instead. Deconvolutions of the ^{29}Si MAS NMR spectra have also been performed without including Q^n components related to Al substitution into paired sites, because Q^1(1Al) units are not often observed in published ^{29}Si MAS NMR spectra of calcium silicate hydrate-based gels,[2; 7; 17; 22; 50] and also because inclusion of these additional Q^n components (Q^1(1Al), Q^2(2Al) and Q^3(2Al) species) would lead to an underconstrained deconvolution procedure. This band at -74 ppm has been observed previously in sodium silicate-activated slag cements,[18] where (similar to the conclusion reached here) it was assigned to Q^0 units, but no strongly established assignment for this peak to a specific site environment within the AAS cement phase assemblage currently exists.

3.3. ^{27}Al MAS NMR spectroscopy

Three distinct Al environments (Al[4], Al[5] and Al[6]) are observed in the ^{27}Al MAS NMR spectra (Figure 7), at δ_{obs} = 52-80 ppm (i.e. the observed chemical shift), 30-40 ppm and 0-20 ppm, respectively.[23] The profiles of the experimental spectra remain similar as the duration of curing increases, but some variation in all three environments is observed between 1-180 days, including:

i) formation of two distinct Al[4] sites at δ_{obs} = 74 ppm and 68 ppm, which is consistent with the dissolution of the slag and the formation of aluminosilicate reaction products;

ii) an increase in the concentration of Al[5] sites, and a sharpening of the peaks corresponding to Al[5] with increasing curing time; and

iii) the increased sharpness and intensity of the Al[6] peak at δ_{obs} = 4 ppm.

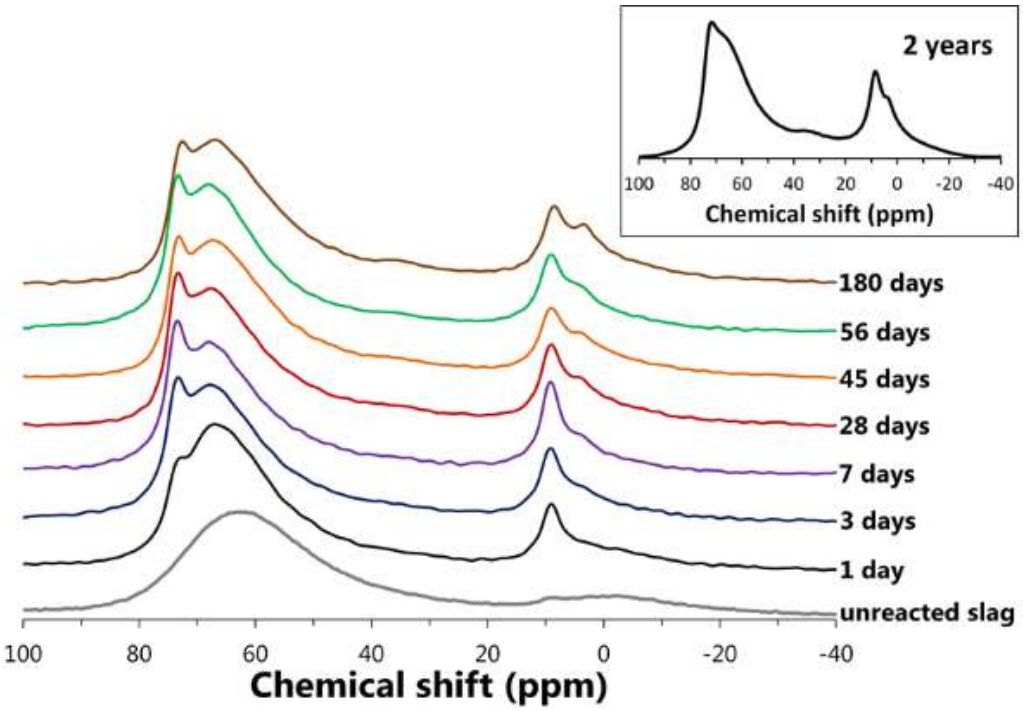

Figure 7. ^{27}Al MAS NMR spectra of the Na_2SiO_3-activated slag paste up to 180 days of curing (14.1 T, ν_R=10 kHz) and the spectrum for the sample cured for 2 years (9.4 T, ν_R=14 kHz).

The four-coordinated Al environments are assigned to the remnant slag particles in the AAS cement, according to the spectrum of the unreacted slag, and also to C-(N-)A-S-H gel. Three distinct Al sites in the C-(N-)A-S-H gel are identified at δ_{obs} = 74 ppm, 68 ppm and 62 ppm (δ_{iso} = 75 ppm, 68 ppm and 62 ppm respectively), in agreement with the literature.[2; 3; 5] The peaks present in the Al[6] region are assigned to hydrotalcite at δ_{obs} = 9.3 ppm and 5.9 ppm (δ_{iso} = 9.68 ppm and 9.1 ppm respectively),[28; 51] which is consistent with the observation of this phase in the XRD results (Figure 1), as well as the third aluminate hydrate (TAH) at δ_{obs} = 3.9 ppm (δ_{iso} = 4.6 ppm). Contributions from TAH are evident because the sharp lineshape of the δ_{obs} ≈ 4 ppm peak cannot be described as hydrotalcite alone.

The quadrupolar coupling parameters used to describe the component peak shapes for the reaction products in the ^{27}Al MAS NMR deconvoluted spectra and the quantified site fractions for these phases are reported in Table 3 and illustrated in Figure 8 for the sample cured for 180 days. Full spectral deconvolutions and fits for each sample are supplied in the Supporting Information. Accurate descriptions of the quadrupolar coupling effects [27] in these phases are typically absent in the alkali-activated cement chemistry literature (where Gaussian/Lorentzian peak shapes are often assumed, even for quadrupolar nuclei), despite the importance of the quadrupolar coupling parameter in determining the component peak shapes and hence intensities, although quadrupolar effects have been accounted for in analysis of ^{27}Al MAS NMR spectra for hydrated PC-based materials [27; 52] and laboratory synthesised C-A-S-H.[5] It is therefore noteworthy that the ^{27}Al MAS NMR spectral deconvolutions presented here provide a greatly enhanced description of the experimental spectra. The proposed peak assignments (where the q^n notation for Al sites is equivalent to the Q^n notation for Si sites[53]) are also consistent with the phases identified through XRD (Figure 1).

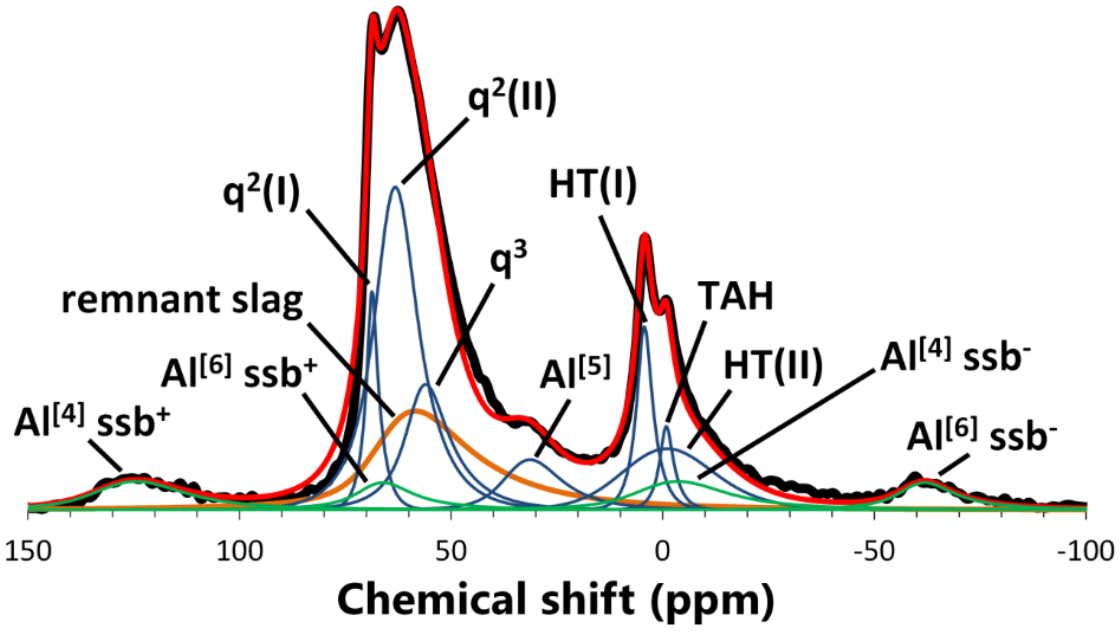

Figure 8. Deconvoluted ^{27}Al MAS NMR spectrum of the Na_2SiO_3-activated slag paste cured for 180 days (14.1 T, ν_R=10 kHz). The contribution of the remnant slag is directly scaled according to the extent of reaction defined from the ^{29}Si MAS NMR spectra. The green sub-peaks are spinning sidebands, and the red line is the sum of the deconvoluted components of the spectrum. Deconvolutions of the spectra obtained at other ages are provided in Appendix B.

336

The ^{27}Al MAS NMR deconvolution results (Table 3) show that hydrotalcite is the dominant Al[6]-containing phase at all ages, which is consistent with the prominent reflections for this phase in the XRD results (Figure 1). Contributions from hydrotalcite are represented by two asymmetric peaks here (marked as HT(I) and HT(II) in Figure 8 and Table 3), to match the known spectrum of this phase.[28; 51] Here, the HT(II) site (δ_{iso} = 9.1 ppm) is assigned specifically to octahedral Al in hydrotalcite that are coordinated to CO_3^{2-} as the interlayer charge-compensating anion,[28] whereas the HT(I) site (δ_{iso} = 9.68 ppm) is assigned to contain contributions from octahedral Al bonded to OH^- in addition to CO_3^{2-}. Despite careful handling and preparation to minimise carbonation of the paste specimen, the XRD results (Figure 1) do show that the samples were slightly carbonated, and recent results by Bernal et al. [33], which suggest that carbonation of hydrotalcite occurs preferentially to the other reaction products in AAS cements, indicates that the hydrotalcite phases formed here may contain carbonate species. The deconvolution results show that the intensity of the HT(II) band is generally greater relative to the HT(I) peak at advanced ages of curing, which is also consistent with the assignment made here because it is reasonable to expect that the specimens are slightly more carbonated at later times of curing. However, the isotropic chemical shift of the reference HT(I) peak and the HT(II) band are 2-3 ppm lower than the reported values of δ_{iso} = 11.8 ppm [28] and δ_{iso} = 11 ppm,[51] meaning that this assignment cannot be made unequivocally.

The q^2 aluminate species at δ_{obs} = 74 and 68 ppm are assigned to two different local environments, q^2(I) and q^2(II) respectively, with lower electron density in the q^2(I) site. The q^2(I) peaks are significantly narrower (Figure 8), suggesting more ordered environments in these sites. Earlier studies have assigned this site to Al substituted into paired tetrahedra in C-A-S-H;[5] however, this site has been left to the more general q^2(I) assignment here, analogously to the Q^1(I) and Q^1(II) silicate sites discussed above. The peak widths of the specific site types are also likely to be affected by the disorder of the aluminosilicate chains in C-(N-)A-S-H gel.[54] The q^2(II) site is assigned to Al[4] in bridging sites of the aluminosilicate chains in C-(N-)A-S-H gel (Figure 5).[5; 55]

The deconvolutions show significant intensity at chemical shifts corresponding to q^3 (and possibly q^4) coordinated Al (δ_{iso} = 62 ppm), suggesting high levels of cross-linking in the C-(N-)A-S-H gel. This is consistent with the literature for silicate-activated slag cements.[32; 38] It is expected that this site contains overlapping contributions from q^3 units with different charge-balancing environments, similar to the situation discussed above for the q^2(I), q^2(II), Q^1(I) and Q^1(II) sites, and potentially also from q^4 sites. These are expected given the assignment of Q^4(3Al) and Q^4(4Al) silicate units in the ^{29}Si MAS NMR spectral deconvolutions. However, quantification of q^4 sites in the deconvoluted ^{27}Al MAS NMR spectra has not been performed here because the deconvolution becomes underconstrained with the inclusion of an additional q^4 peak.

The evolving nature of the Al environments in the AAS cement can be illustrated by normalizing the reaction product intensities to 100% and removing the contributions attributed to the remnant slag component (Figure 9), comparable to Figure 6 describing Si environments. The relative intensities assigned to the q^3 (and possibly q^4) and q^2 sites, and the HT(I) and HT(II) sites, have also been combined in Figure 9 because these site environments are not yet well defined in AAS cements.

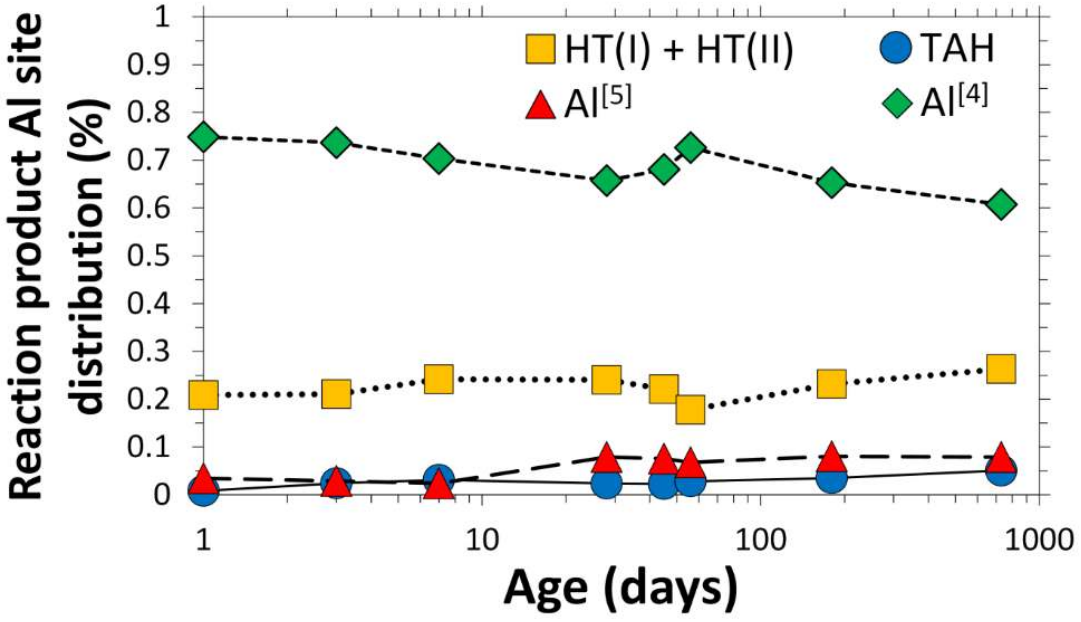

Figure 9. Deconvolution results for the ^{27}Al MAS NMR spectra normalized to the total intensity of the reaction products as a function of the time of curing. Samples aged for 1-180 days were measured at 14.1 T, ν_R=10 kHz, and the sample cured for 2 years was measured at 9.4 T, ν_R=14 kHz.

In general, the normalized ^{27}Al MAS NMR spectral deconvolution results (Figure 9) show that as curing time increases, the relative percentage of Al[4] environments in the solid binder decreases and the combined relative intensity of the HT peaks remain approximately constant. The intensity of the TAH and Al[5] peaks increase as a function of curing time. Here, Al[5] is tentatively assigned to interlayer species in the C-(N-)A-S-H gel that charge-balance the aluminosilicate chains present in this phase.[2; 20; 56] The increased amount of this component at 28 days and later in the ^{27}Al MAS NMR spectra is consistent with experimental ^{27}Al MAS NMR spectra of AAS cements,[6; 8] laboratory-synthesised C-(N-)A-S-H gels,[2; 3] and PC-based materials. [20; 56; 57]

No clear contributions from AFm or hydrogarnet are observed in the ^{27}Al MAS NMR spectra, which is consistent with the absence of prominent reflections corresponding to these phases in the XRD results (Figure 1). These results indicate that the solid phase assemblage varies only slightly between 1 day and 2 years of curing (noting again that the effect of the extent of reaction has been removed from these data), with the exception of the appearance of a small amount of N-A-S(-H) gel at 56 days and later, as discussed in section 3.2.

3.4. Characterisation of the C-(N-)A-S-H gel

The deconvoluted ^{29}Si MAS NMR spectra (Table 2) are analyzed using the CSTM structural description of cross-linking in tobermorite-type gels,[16] to characterize the chemistry and structure of the C-(N-)A-S-H gel formed here (Table 4).

401 Fixed values of interlayer calcium content (ω=φ=0.25) were used in the model to match the average
402 binder composition (Ca/Si and Ca/(Al+Si)) of this AAS cement measured by environmental scanning
403 electron microscopy with energy-dispersive X-ray spectroscopy (ESEM-EDS) as a function of curing
404 time.[16] The structure of the C-(N-)A-S-H gel is mostly cross-linked between 1-180 days, despite the low
405 apparent intensity of the Q^3(1Al) component in the deconvoluted ^{29}Si MAS NMR spectra (Table 2). The
406 Al/Si ratio of the C-(N-)A-S-H gel decreases slightly as curing time increases, reflecting the reduction in
407 the relative Q^2(1Al), Q^3(1Al) and Al[4] site percentages (Figures 6 and 9). The decreasing fraction of
408 the cross-linked component of the gel at later ages is a consequence of the relative reduction in
409 Q^3(1Al) sites and the formation of the additional disordered (Q^4 and possibly q^4 containing) activation
410 product at extended ages. A similar decreasing trend in MCL is found with increasing curing time,
411 indicating that the cross-linked phase fraction – so also the intensities of the Q^3(1Al) sites and the
412 formation of the additional Q^4-containing product – are the key parameters influencing the extent of
413 polymerization of the partially cross-linked C-(N-)A-S-H gels characterized here. The Ca/Si ratio of the
414 binder was not found to increase from 7 to 56 days by ESEM-EDS,[16] in support of this analysis. The
415 percentage of Al in the cross-linked component of the gel is between 40-60 % at all curing times, which
416 suggests that Al substitutes into both cross-linked and non-cross-linked components of C-(N-)A-S-H
417 gels without a clear preference for either structural type.

418 The percentages of Al in the cross-linked gel components are calculated according to eq.(1):

419
$$\%Al_{[C]} = 100\frac{\left(Al/Si\right)_{[C]}\left[Q^1 + Q^2(1Al) + Q^2 + Q^3(1Al) + Q^3\right]_{[C]}}{\sum_k\left(\left(Al/Si\right)_k\left[Q^1 + Q^2(1Al) + Q^2 + Q^3(1Al) + Q^3\right]_k\right)} \quad (1)$$

420 where the subscripts $[C]$ and $[NC]$ represent the cross-linked and non-cross-linked components of the
421 C-(N-)A-S-H gel respectively, $k \in \{[C],[NC]\}$, the Q^n site fractions are taken from the ^{29}Si MAS NMR
422 spectral deconvolution results (Table 2), and $(Al/Si)_{[C]}$ and $(Al/Si)_{[NC]}$ are defined by eqs.(2-3):

$$\left(Al/Si\right)_{[C]} = \frac{Q^3(1Al)}{Q^1 + Q^2 + Q^2\left(1Al\right) + Q^3 + Q^3\left(1Al\right)} \quad (2)$$

$$\left(Al/Si\right)_{[NC]} = \frac{\left(\frac{1}{2}\right)Q^2(1Al)}{Q^1 + Q^2 + Q^2(1Al)} \quad (3)$$

Maximum partitioning of Q^1 units into the cross-linked component of the gel ($\eta \rightarrow \eta_{max}$) was specified because the MCL and Al/Si ratio of this phase are similar (MCL ≈ 10 and Al/Si ≈ 0.11) at all values of η that satisfy the structural constraints of the gel,[16] for the C-(N-)A-S-H gel formed here. Partitioning of Q^1 sites can be defined differently (e.g. specifying the minimum value of η that satisfies the structural constraints of the gel), but as long as the method used is consistent, the structural trends obtained from the CSTM are the same. Hence the trends related to the structure of the C-(N-)A-S-H gel, rather than the absolute values, are the key targets for analysis. The choice of η does not affect the calculated overall Al/Si ratio of the C-(N-)A-S-H gel or the concentration of Al in the cross-linked component of the gel.

A strong link between the Al content and MCL of the C-(N-)A-S-H gel is found by distinguishing the cross-linked and non-cross-linked components of the gel (Table 4). This is a consequence of the low capacity of cross-linked C-(N-)A-S-H structures to incorporate Al, as illustrated by Figure 5: only one in each six tetrahedral sites in cross-linked C-(N-)A-S-H units can accommodate Al, compared to one in three tetrahedral sites in non-cross-linked C-(N-)A-S-H units. The data in Table 4 indicate that if the average Al/Si ratio of the C-(N-)A-S-H gel is significantly greater than 0.11 (the Al/Si ratio of Al-saturated, MCL = 10 cross-linked tobermorite), then the non-cross-linked chain structures are significantly more polymerized and Al-rich than the C-(N-)A-S-H gel as a whole, because these structures must incorporate all of the remaining Al. Therefore, small variations in the overall Al/Si ratio of the C-(N-)A-S-H gel can lead to major structural and chemical changes in the non-cross-linked component of C-(N-)A-S-H gels, meaning that significant variations in the structure and chemistry of the C-(N-)A-S-H gel can be expected in AAS cements of superficially similar composition.

3.5. Perspectives

This new understanding of C-(N-)A-S-H gel further highlights the importance of a fundamental scientific approach to the design and formulation of modern cement materials. The relationship between structure and Al content in C-(N-)A-S-H may be important in determining the mechanical and thermodynamic properties of blended PC/Al-containing SCM materials and alkali-activated cements. The results presented here strongly indicate that single-phase structural representations of C-(N-)A-S-H gel are insufficient to accurately characterize the chemical composition and structure of this phase; multi-phase models for C-(N-)A-S-H gels [15; 58] should be used to describe these materials.

However, because the CSTM does not embody a description of the Q^4-containing disordered aluminosilicate phase, separate quantification is needed. Here, this phase is discussed as resembling an intimately-mixed zeolite-like phase similar to the N-A-S(-H) gels formed through the alkali-activation of low-calcium aluminosilicate precursors,[39] which was quantified from the ^{29}Si MAS NMR spectral deconvolutions, enabling use of the CSTM to fully characterise the structure and chemistry of the C-(N-)A-S-H gel formed here. It may also possibly be described as a degradation product of carbonated C-(N-)A-S-H gel, although the application of multinuclear NMR techniques to better distinguish the $Q^n(m\text{Al})$ environments in the solid binder seems to be essential in further refining the understanding in this area. The identification of this disordered aluminosilicate phase also indicates a need to understand the structural relationship(s) of this phase in the solid binder, as it is known that the phase stability of calcium-deficient sodium-aluminosilicate gels and C-(N-)A-S-H gels differ significantly.[59]

4. Conclusions

Spectroscopic and diffractometric analysis of the nanostructural development of a sodium silicate-activated slag cement up to 180 days of curing shows the presence of a dominant C-(N-)A-S-H gel, with hydrotalcite and TAH secondary products. Five-coordinated Al, tentatively assigned to interlayer charge-balancing species in the C-(N-)A-S-H gel, was also observed at all ages.

Application of the 'Cross-linked Substituted Tobermorite Model', describing mixed cross-linked/non-cross-linked tobermorite-like structures, showed decreasing trends in the MCL, extent of cross-linking and Al/Si ratio of the C-(N-)A-S-H gel over time. The C-(N-)A-S-H gel was highly cross-linked despite the low relative intensity of Q^3(1Al) sites, and an additional highly-polymerized aluminosilicate phase, containing Q^4(3Al) and Q^4(4Al) sites and proposed here to potentially resemble the nanocrystalline products found in calcium-deficient sodium-aluminosilicate hydrate ('geopolymer') gels, was required for consistency with the spectra collected at later ages. This has important implications for understanding the durability of AAS cement-based materials, as the phase stabilities of geopolymer gels and C-(N-)A-S-H gels are known to differ significantly. The chemical and structural nature of the C-(N-)A-S-H gel varied significantly across a relatively narrow range of chemical compositions. A complex relationship exists between the Al content and the extent of polymerization of the C-(N-)A-S-H gels, due to the lower relative capacity of cross-linked C-(N-)A-S-H to structurally incorporate Al. Increasing the Al content of cross-linked C-(N-)A-S-H gels may not necessarily induce increased polymerization.

These results, and the methods for analysis of ^{29}Si and ^{27}Al MAS NMR spectra developed here, will have significant implications for the ways in which AAS cements and blended PC/Al-containing SCM materials are described, understood and modeled.

5. Supporting information

Additional material is provided as Electronic Supporting Information: the quantification procedure for the ^{27}Al MAS NMR spectra is provided in Appendix A; deconvoluted ^{29}Si MAS NMR spectra (Figure S1) and deconvoluted ^{27}Al MAS NMR spectra (Figures S2 and S3) are presented in Appendix B; and detailed discussion regarding the deconvolutions of bands at -93 ppm and -89 ppm in the ^{29}Si MAS NMR spectra is provided in Appendix C.

6. Acknowledgements

This work was funded in part by the Australian Research Council (ARC), including support through a Linkage Project co-funded by Zeobond Pty Ltd, and through the Particulate Fluids Processing Centre, a Special Research Centre of the ARC. Funding support provided by the University of Sheffield is also gratefully acknowledged. We thank Sam A. Walling (University of Sheffield) for sharing important results regarding the NMR analysis of hydrotalcite.

7. References

1. B. Lothenbach, K. Scrivener, and R. D. Hooton, "Supplementary cementitious materials", *Cem. Concr. Res.,* **41**[12], 1244-1256 (2011).

2. G. K. Sun, J. F. Young, and R. J. Kirkpatrick, "The role of Al in C-S-H: NMR, XRD, and compositional results for precipitated samples", *Cem. Concr. Res.,* **36**[1], 18-29 (2006).

3. P. Faucon, A. Delagrave, J. C. Petit, C. Richet, J. M. Marchand, and H. Zanni, "Aluminum incorporation in calcium silicate hydrates (C-S-H) depending on their Ca/Si ratio", *J. Phys. Chem. B,* **103**[37], 7796-7802 (1999).

4. G. Renaudin, J. Russias, F. Leroux, C. Cau Dit Coumes, and F. Frizon, "Structural characterization of C-S-H and C-A-S-H samples - part II: local environment investigated by spectroscopic analyses", *J. Solid State Chem.,* **182**[12], 3320-3329 (2009).

5. X. Pardal, F. Brunet, T. Charpentier, I. Pochard, and A. Nonat, "^{27}Al and ^{29}Si solid-state NMR characterization of calcium-aluminosilicate-hydrate", *Inorg. Chem.,* **51**[3], 1827-1836 (2012).

6. I. G. Richardson, A. R. Brough, G. W. Groves, and C. M. Dobson, "The characterization of hardened alkali-activated blast-furnace slag pastes and the nature of the calcium silicate hydrate (C-S-H) phase", *Cem. Concr. Res.,* **24**[5], 813-829 (1994).

7. S. D. Wang and K. L. Scrivener, "^{29}Si and ^{27}Al NMR study of alkali-activated slag", *Cem. Concr. Res.,* **33**[5], 769-774 (2003).

8. F. Bonk, J. Schneider, M. A. Cincotto, and H. Panepucci, "Characterization by multinuclear high-resolution NMR of hydration products in activated blast-furnace slag pastes", *J. Am. Ceram. Soc.,* **86**[10], 1712-1719 (2003).

9. M. C. G. Juenger, F. Winnefeld, J. L. Provis, and J. H. Ideker, "Advances in alternative cementitious binders", *Cem. Concr. Res.,* **41**[12], 1232-1243 (2011).

10. S. A. Bernal and J. L. Provis, "Durability of alkali-activated materials: progress and perspectives", *J. Am. Ceram. Soc.,* **97**[4], 997-1008 (2014).

11. J. L. Provis, R. J. Myers, C. E. White, V. Rose, and J. S. J. van Deventer, "X-ray microtomography shows pore structure and tortuosity in alkali-activated binders", *Cem. Concr. Res.,* **42**[6], 855-864 (2012).

12. S. Y. Hong and F. P. Glasser, "Alkali sorption by C-S-H and C-A-S-H gels: part II. Role of alumina", *Cem. Concr. Res.,* **32**[7], 1101-1111 (2002).

13. J. Skibsted and M. D. Andersen, "The effect of alkali ions on the incorporation of aluminum in the calcium silicate hydrate (C–S–H) phase resulting from Portland cement hydration studied by ^{29}Si MAS NMR", *J. Am. Ceram. Soc.,* **96**, 651-656 (2013).

14. L. B. Skinner, S. R. Chae, C. J. Benmore, H. R. Wenk, and P. J. M. Monteiro, "Nanostructure of calcium silicate hydrates in cements", *Phys. Rev. Lett.,* **104**[195502], 1-4 (2010).

15. F. Puertas, M. Palacios, H. Manzano, J. S. Dolado, A. Rico, and J. Rodríguez, "A model for the C-A-S-H gel formed in alkali-activated slag cements", *J. Eur. Ceram. Soc.,* **31**[12], 2043-2056 (2011).

16. R. J. Myers, S. A. Bernal, R. San Nicolas, and J. L. Provis, "Generalized structural description of calcium-sodium aluminosilicate hydrate gels: the cross-linked substituted tobermorite model", *Langmuir,* **29**, 5294-5306 (2013).

17. A. R. Brough and A. Atkinson, "Sodium silicate-based, alkali-activated slag mortars - part I. Strength, hydration and microstructure", *Cem. Concr. Res.,* **32**[6], 865-879 (2002).

18. G. Le Saoût, M. Ben Haha, F. Winnefeld, and B. Lothenbach, "Hydration degree of alkali-activated slags: a ^{29}Si NMR study", *J. Am. Ceram. Soc.,* **94**[12], 4541-4547 (2011).

19. L. Pegado, C. Labbez, and S. V. Churakov, "Mechanism of aluminium incorporation into C-S-H from ab initio calculations", *J. Mater. Chem. A,* **2**[10], 3477-3483 (2014).

20. M. D. Andersen, H. J. Jakobsen, and J. Skibsted, "A new aluminium-hydrate species in hydrated Portland cements characterized by ^{27}Al and ^{29}Si MAS NMR spectroscopy", *Cem. Concr. Res.,* **36**[1], 3-17 (2006).

21. G. Engelhardt and H. Koller, "A simple procedure for the determination of the quadrupole interaction parameters and isotropic chemical shifts from magic angle spinning NMR spectra of half-integer spin nuclei in solids", *Magn. Reson. Chem.,* **29**[9], 941-945 (1991).

22. I. G. Richardson, A. R. Brough, R. Brydson, G. W. Groves, and C. M. Dobson, "Location of aluminum in substituted calcium silicate hydrate (C-S-H) gels as determined by ^{29}Si and ^{27}Al NMR and EELS", *J. Am. Ceram. Soc.,* **76**[9], 2285-2288 (1993).

23. G. Engelhardt and D. Michel, "High-Resolution Solid-State NMR of Silicates and Zeolites". John Wiley & Sons, Chichester, 1987.

24. S. A. Bernal, J. L. Provis, B. Walkley, R. San Nicolas, J. G. Gehman, D. G. Brice, A. Kilcullen, P. Duxson, and J. S. J. van Deventer, "Gel nanostructure in akali-activated binders based on slag and fly ash, and effects of accelerated carbonation", *Cem. Concr. Res.,* **53**, 127-144 (2013).

25. D. Massiot, F. Fayon, M. Capron, I. King, S. Le Calvé, B. Alonso, J.-O. Durand, B. Bujoli, Z. Gan, and G. Hoatson, "Modelling one- and two-dimensional solid-state NMR spectra", *Magn. Reson. Chem.,* **40**[1], 70-76 (2002).

570 26. D. R. Neuville, L. Cormier, and D. Massiot, "Al environment in tectosilicate and peraluminous
571 glasses: a ^{27}Al MG-MAS NMR, Raman, and XANES investigation", *Geochim. Cosmochim. Acta,*
572 **68**[24], 5071-5079 (2004).

573 27. J.-B. d'Espinose de Lacaillerie, C. Fretigny, and D. Massiot, "MAS NMR spectra of quadrupolar
574 nuclei in disordered solids: the Czjzek model", *J. Magn. Reson.,* **192**[2], 244-251 (2008).

575 28. P. J. Sideris, F. Blanc, Z. Gan, and C. P. Grey, "Identification of cation clustering in Mg–Al layered
576 double hydroxides using multinuclear solid state nuclear magnetic resonance spectroscopy",
577 *Chem. Mater.,* **24**[13], 2449-2461 (2012).

578 29. A. Fernández-Jiménez and F. Puertas, "Effect of activator mix on the hydration and strength
579 behaviour of alkali-activated slag cements", *Adv. Cem. Res.,* **15**[3], 129-136 (2003).

580 30. S. D. Wang and K. L. Scrivener, "Hydration products of alkali activated slag cement", *Cem.*
581 *Concr. Res.,* **25**[3], 561-571 (1995).

582 31. M. Ben Haha, B. Lothenbach, G. Le Saoût, and F. Winnefeld, "Influence of slag chemistry on
583 the hydration of alkali-activated blast-furnace slag - part I: effect of MgO", *Cem. Concr. Res.,*
584 **41**[9], 955-963 (2011).

585 32. A. Fernández-Jiménez, F. Puertas, I. Sobrados, and J. Sanz, "Structure of calcium silicate
586 hydrates formed in alkaline-activated slag: Influence of the type of alkaline activator", *J. Am.*
587 *Ceram. Soc.,* **86**[8], 1389-1394 (2003).

588 33. S. A. Bernal, R. San Nicolas, R. J. Myers, R. Mejía de Gutiérrez, F. Puertas, J. S. J. van Deventer,
589 and J. L. Provis, "MgO content of slag controls phase evolution and structural changes induced
590 by accelerated carbonation in alkali-activated binders", *Cem. Concr. Res.,* **57**, 33-43 (2014).

591 34. R. J. Kirkpatrick, "MAS NMR-spectroscopy of minerals and glasses", *Rev. Mineral.,* **18**, 341-403
592 (1988).

593 35. J. Schneider, M. A. Cincotto, and H. Panepucci, "^{29}Si and ^{27}Al high-resolution NMR
594 characterization of calcium silicate hydrate phases in activated blast-furnace slag pastes",
595 *Cem. Concr. Res.,* **31**[7], 993-1001 (2001).

596 36. P. Rejmak, J. S. Dolado, M. J. Stott, and A. Ayuela, "^{29}Si NMR in cement: a theoretical study on
597 calcium silicate hydrates", *J. Phys. Chem. C,* **116**[17], 9755-9761 (2012).

37. J. L. Provis, P. Duxson, G. C. Lukey, and J. S. J. Van Deventer, "Statistical thermodynamic model for Si/Al ordering in amorphous aluminosilicates", *Chem. Mater.,* **17**[11], 2976-2986 (2005).

38. M. Palacios and F. Puertas, "Effect of carbonation on alkali-activated slag paste", *J. Am. Ceram. Soc.,* **89**[10], 3211-3221 (2006).

39. J. L. Provis, G. C. Lukey, and J. S. J. van Deventer, "Do geopolymers actually contain nanocrystalline zeolites? A reexamination of existing results", *Chem. Mater.,* **17**[12], 3075-3085 (2005).

40. J. L. Bell, P. Sarin, J. L. Provis, R. P. Haggerty, P. E. Driemeyer, P. J. Chupas, J. S. J. van Deventer, and W. M. Kriven, "Atomic Structure of a Cesium Aluminosilicate Geopolymer: A Pair Distribution Function Study", *Chem. Mater.,* **20**[14], 4768-4776 (2008).

41. S. A. Bernal, J. L. Provis, R. Mejía de Gutierrez, and V. Rose, "Evolution of binder structure in sodium silicate-activated slag-metakaolin blends", *Cem. Concr. Compos.,* **33**[1], 46-54 (2011).

42. S. A. Bernal, J. L. Provis, V. Rose, and R. Mejía de Gutiérrez, "High-resolution X-ray diffraction and fluorescence microscopy characterization of alkali-activated slag-metakaolin binders", *J. Am. Ceram. Soc.,* **96**[6], 1951-1957 (2013).

43. J. L. Provis and S. A. Bernal, "Geopolymers and related alkali-activated materials", *Annu. Rev. Mater. Res.,* **44**, 299-327 (2014).

44. M. Ben Haha, G. Le Saoût, F. Winnefeld, and B. Lothenbach, "Influence of activator type on hydration kinetics, hydrate assemblage and microstructural development of alkali activated blast-furnace slags", *Cem. Concr. Res.,* **41**[3], 301-310 (2011).

45. V. Kocaba, E. Gallucci, and K. L. Scrivener, "Methods for determination of degree of reaction of slag in blended cement pastes", *Cem. Concr. Res.,* **42**[3], 511-525 (2012).

46. P. Duxson, J. L. Provis, G. C. Lukey, F. Separovic, and J. S. J. van Deventer, "^{29}Si NMR study of structural ordering in aluminosilicate geopolymer gels", *Langmuir,* **21**[7], 3028-3036 (2005).

47. I. G. Richardson, "Tobermorite/jennite- and tobermorite/calcium hydroxide-based models for the structure of C-S-H: applicability to hardened pastes of tricalcium silicate, β-dicalcium silicate, Portland cement, and blends of Portland cement with blast-furnace slag, metakaolin, or silica fume", *Cem. Concr. Res.,* **34**[9], 1733-1777 (2004).

48. M. J. Abdolhosseini Qomi, F. J. Ulm, and R. J. M. Pellenq, "Evidence on the dual nature of aluminum in the calcium-silicate-hydrates based on atomistic simulations", *J. Am. Ceram. Soc.,* **95**[3], 1128-1137 (2012).

49. H. Manzano, J. S. Dolado, and A. Ayuela, "Aluminum incorporation to dreierketten silicate chains", *J. Phys. Chem. B,* **113**[9], 2832-2839 (2009).

50. P. J. Schilling, L. G. Butler, A. Roy, and H. C. Eaton, "^{29}Si and ^{27}Al MAS-NMR of NaOH-activated blast-furnace slag", *J. Am. Ceram. Soc.,* **77**[9], 2363-2368 (1994).

51. A. Vyalikh, D. Massiot, and U. Scheler, "Structural characterisation of aluminium layered double hydroxides by ^{27}Al solid-state NMR", *Solid State Nucl. Mag.,* **36**[1], 19-23 (2009).

52. T. T. H. Bach, C. C. D. Coumes, I. Pochard, C. Mercier, B. Revel, and A. Nonat, "Influence of temperature on the hydration products of low pH cements", *Cem. Concr. Res.,* **42**[6], 805-817 (2012).

53. R. K. Harris, A. Samadi-Maybodi, and W. Smith, "The incorporation of aluminum into silicate ions in alkaline aqueous solutions, studied by ^{27}Al NMR", *Zeolites,* **19**[2–3], 147-155 (1997).

54. H. F. W. Taylor, "Cement Chemistry". Thomas Telford Publishing, London, 1997.

55. J. Houston, R. Maxwell, and S. Carroll, "Transformation of meta-stable calcium silicate hydrates to tobermorite: reaction kinetics and molecular structure from XRD and NMR spectroscopy", *Geochem. Trans.,* **10**[1], 1 (2009).

56. C. A. Love, I. G. Richardson, and A. R. Brough, "Composition and structure of C–S–H in white Portland cement–20% metakaolin pastes hydrated at 25 °C", *Cem. Concr. Res.,* **37**[2], 109-117 (2007).

57. R. Taylor, I. G. Richardson, and R. M. D. Brydson, "Composition and microstructure of 20-year-old ordinary Portland cement-ground granulated blast-furnace slag blends containing 0 to 100% slag", *Cem. Concr. Res.,* **40**[7], 971-983 (2010).

58. D. A. Kulik, "Improving the structural consistency of C-S-H solid solution thermodynamic models", *Cem. Concr. Res.,* **41**[5], 477-495 (2011).

59. J. S. J. van Deventer, J. L. Provis, and P. Duxson, "Technical and commercial progress in the adoption of geopolymer cement", *Miner. Eng.,* **29**, 89-104 (2012).

654

655